Supplementary Information

Separator Rich in SnF_2 and NO_3^- Direct Ultra-Stable Interface toward High Performance Li Metal Batteries

Yucheng Wen‡[a] Jieying Ding,‡[a] Jun Liu,[a] Min Zhu,[a] and Renzong Hu*[a]

[a] School of Materials Science and Engineering, Guangdong Provincial Key Laboratory of Advanced Energy Storage Materials, South China University of Technology, Guangzhou, 510640, China. E-mail: msrenzonghu@scut.edu.cn

‡ These authors contributed equally: Yucheng Wen and Jieying Ding

Methods

Synthesis of nano-SnF_2. Firstly, $SnBr_2$ and NH_4F were dissolved in methanol, followed by adding NH_4F solution to $SnBr_2$ solution under an ice water bath, stirring continuously for 10 hours. Then, the product was washed with methanol 3 times, and eventually dried under vacuum at 80℃ for 12 hours to obtain the target product.

Synthesis of EB-COF:NO_3@SnF_2. Firstly, 0.4 mmol 1, 3, 5-triformylphloroglucinol (TFP), 0.6 mmol ethidium bromide (EB) and 20 mg nano-SnF_2 were dissolved in 2 ml of solution of 1, 4-dioxane mesitylene (v/v=1:1) with 0.4 ml 6 mol L^{-1} acetic acid added. Subsequently, in a quartz conical flask, the mixture reacts at 120°C for 72 h under an argon atmosphere to obtain a dark crimson solid. Next, after washing 3 times with 1, 4-dioxane, tetrahydrofuran, and anhydrous ethanol, the precursor was produced by drying for 12 hours in a vacuum oven at 85°C. Then, the obtained precursor (1.5 g) was disseminated in a 15 mL saturated lithium nitrate solution of methanol. The residue was filtered after the solution was constantly agitated for 24 h. To acquire the goal product, repeat the preceding method 5 times, afterwards wash the final precipitate 3 times with H_2O. Shanghai Aladdin Bio-Chem Technology Co., LTD in China provided these chemical reagents.

Synthesis of PCS. The synthesized EB-COF:NO_3@SnF_2 and polyvinylidene difluoride (PVDF) (90 : 10 in wt%) were dispersed in N-Methylpyrrolidone (NMP) for forming a slurry at room temperature. Next, the slurry was coated on a polypropylene separator,

and subsequently dry it at 60℃ for 12 h in a vacuum. Finally, the procured PCS was cut into small pieces for battery assembly.

Electrodes Preparation. The cathode electrodes were obtained by putting $LiNi_{0.8}Co_{0.1}Mn_{0.1}O_2$ or $LiFePO_4$ (LFP, NCM811, Hefei Kejing Materials Technology Co., Ltd. China), carbon black, and PVDF binder in NMP, subsequently coating the slurry onto Al foil, and drying continuously at 120°C in a vacuum oven for 12 h. In this study, the carbonate-based electrolytes (1.0 M lithium hexafluorophosphate ($LiPF_6$) in ethylene carbonate (EC) : ethyl methyl carbonate (EMC) = 3 : 7 in Vol% and 1.0 M lithium oxalyldifluoroborate (LiDFOB) in ethylene carbonate (EC) : ethyl methyl carbonate (EMC) = 3 : 7 in Vol% with 2% Fluoroethylene carbonate (FEC)), the ether-based electrolytes (1.0 M lithium bis((trifluoromethyl)sulfonyl)azanide (LiTFSI) in dimethoxyethane (DME) : 1, 3-dioxolane (DOL) = 1 : 1 in Vol%) and PP (ϕ =18 mm) were provided by Guangzhou Tinci Materials Technology Co. Ltd. China. The Li anode with thickness of 500 μm, 50 μm and 25 μm used in cell tests is purchased from China Energy Lithium Co., Ltd.

Measurements and characterizations. Li//LFP, Li//NCM811, Li//Li and Li//Cu cells (2025 type) were assembled in an argon-filled glove box with moisture and oxygen contents controlled to be less than 1 ppm to evaluate the effectiveness of PCS for high energy density Li metal batteries. The LAND system (CT2001A, China) was used to test charge/discharge cycling on these cells. The Li//LFP full cells were tested with a

voltage range of 2.5 - 4.0 V (vs. Li/Li^+) at 0.2 C (1 C =170 mAh g^{-1}) for the initial 3 cycles and at 0.5 C for the remaining cycles. The Li//NCM811 cells were cycled with a voltage range of 3.0 - 4.2 V, 4.4 V or 4.5 V at 0.3 C (1 C = 200 mAh g^{-1}) for the initial 3 cycles and at 1 C for the remaining cycles, while the rate capacity of that was carried from 0.3 C to 5 C then reverted to 0.3 C. The NCM811 full cell with Cu anode using PCS pre-deposited Li was evaluated under a voltage range of 3 - 4.5 V at 1 C. The current density for pre-deposited Li on Cu using PCS is 0.5 mA cm^{-2} and the capacity is 4 mAh cm^{-2}. The elevated loading Li//NCM811 full cell was tested at a charge current density of 0.2 C and a discharge current density of 0.5 C with a voltage range of 3 - 4.4 V. The Li//NCM811 pouch cell was tested at a charge current density of 0.2 C and a discharge current density of 0.4 C with a voltage range of 3 - 4.4 V. The Li//Li symmetric cells with varying capacities of 2 mAh cm^{-2} and 30 mAh cm^{-2} were assessed at varied current densities of 15 mA cm^{-2} and 10 mA cm^{-2}, respectively. The rate capability of Li//Li symmetric cells was measured at various currents of 0.5, 1, 2, 5 and 10 mA cm^{-2} with a fixed capacity of 1 mAh cm^{-2}. The Li//Cu cells cycled between 0 and 1 V with a current density of 1 mA cm^{-2} to evaluate Coulombic efficiency. The H-type Li//Cu cell performed the deposition process for 20 h under a current of 0.5 mA cm^{-2}. Cyclic voltammetry (CV) of Li//Cu cells was performed at various scan speeds of 0.5 mV s^{-1} throughout the voltage range of -0.2 - 1 V. Tafel plots were acquired in Li symmetric cells with a scan rate of 0.5 mV s^{-1} within a voltage range of -0.2 - 0.2 V and then handled for linear fitting.

On the Gamry Interface 1000 Electrochemical System, electrochemical

impedance spectra (EIS) of Li//NCM811 and Li//Li cells were recorded throughout a frequency range of 10^5 to 10^{-2} Hz and a voltage amplitude of 5 mV. To estimate the ion conductivity (δ), symmetrical stainless steel (ϕ = 16 mm) cells containing PP and PCS were assembled, employing electrochemical impedance with a frequency range from 10^5 to 10^{-1} Hz and voltage amplitude of 5 mV, using the equation (1):

$$\delta = \frac{d}{R_b \times S}$$

where R_b is the bulk resistance, d and *S* are the thickness and area of separator, respectively.

The tortuosity (τ) of separator was measured by the following equation (2):

$$\tau = \sqrt{\varepsilon \times \frac{\delta_0}{\delta_e}}$$

where δ_0 (8.9 mS cm^{-1}) is the ion conductivity of electrolyte, δ_e is the ion conductivity of separator in the electrolyte.

The porosity (ε) of separator was calculated by the following equation (3):

$$\varepsilon = \frac{W_b - W_a}{\rho \times V_0} \times 100\%$$

where W_a and W_b represent the weight of the separator before and after being submerged in the n-butanol, ρ and V_0 represent the density of n-butanol and the volume of the separator, respectively.

Then, the activation energy is calculated by the Arrhenius equation (4):

$$\ln K = -\frac{E_a}{RT} + \ln A$$

To test the Li^+ transference number (t_{Li^+}), the Li symmetric cell was tested with chronoamperometry at a polarization voltage of 10 mV for 2000 s, then calculated according to the following equation (5):

$$t_{Li^+} = \frac{I_s \times (\Delta V - I_i \times R_i)}{I_i \times (\Delta V - I_s \times R_s)}$$

where ΔV represents the polarization voltage, I_i and I_s represent the initial and steady-state currents, and R_i and R_s represent the resistances obtained from the EIS spectra of cell before and after polarization, respectively.

The content change of the element in PCS was detected by the following method using inductively coupled plasma mass spectrometry (ICP-MS, Agilent 7700s). Firstly, 20 ml of concentrated nitric acid was added to the sample in a flask. Next, the sample was continually stirred in a water bath (60℃) until it was completely dissolved. Finally, the sample was diluted 100 times to check the content of the elements. X-ray diffraction (XRD, PANalytical X'Pert Pro Alpha-1) was employed to identify the synthesis of SnF_2 and the crystal structures of NCM811 cathode after cycling. Fourier-transform infrared (FTIR) spectra were obtained from Thermo Scientific Nicolet iS50 FTIR spectrometer. The contact angle test between separator and electrolyte is performed on DSA25E Contact Angle System. The Gurley value of separator was tested from Gurley4110N. Surface morphology and chemical composition were investigated by scanning electron microscopy (SEM, TESCAN GAIA3 model 2016 UHR), transmission electron microscopy (TEM, JEM-2100, JOEL) and x-ray photoelectron spectroscopy (XPS, Thermo Scientific K-Alpha Nexsa). Solid state ^{31}P was used to detect the change of substances in the PCS after cycling. The sample was cut into numerous small pieces and then tested on Agilent 600 DD2 spectrometer (Agilent, USA, magnetic field strength 14.1 T). Morphological and structural information of Li deposits were investigated by cryogenic-transmission electron microscopy (cryo-TEM, Talos 200X)

using ceta cameral cryo-transfer holder. All cryogenic TEM images were captured from low temperatures (-180°C). Before physical characterization, all electrodes were washed with DEC 3 times in the Ar-filled glovebox to wipe off residuary electrolytes.

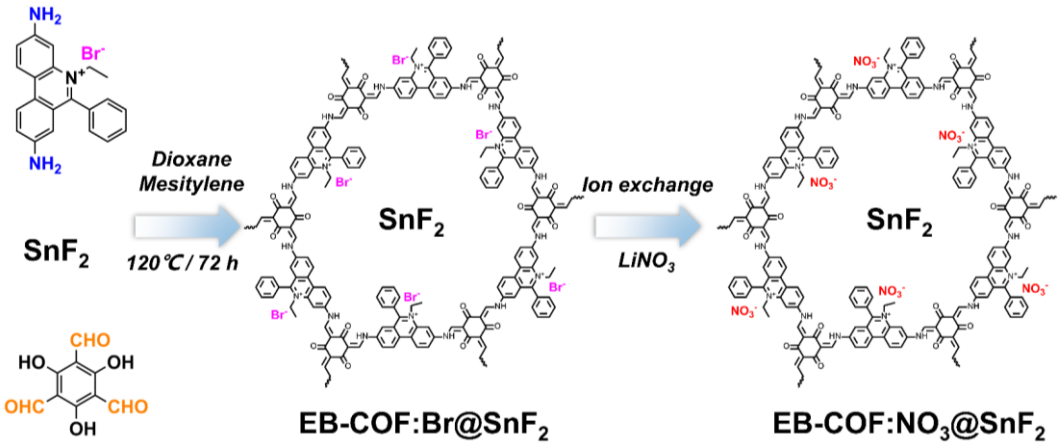

Figure S1. The synthesis route of EB-COF:NO_3@SnF_2.

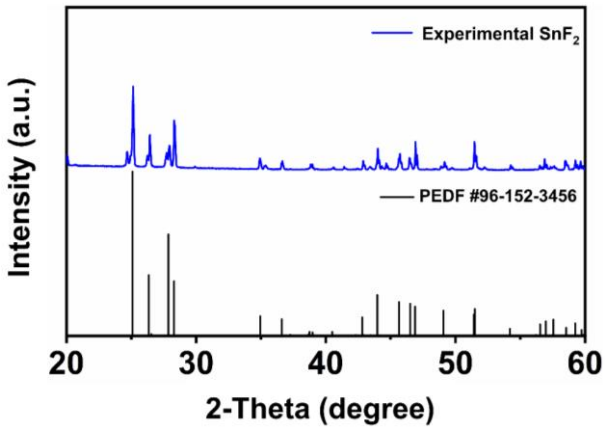

Figure S2. XRD of nano-SnF_2.

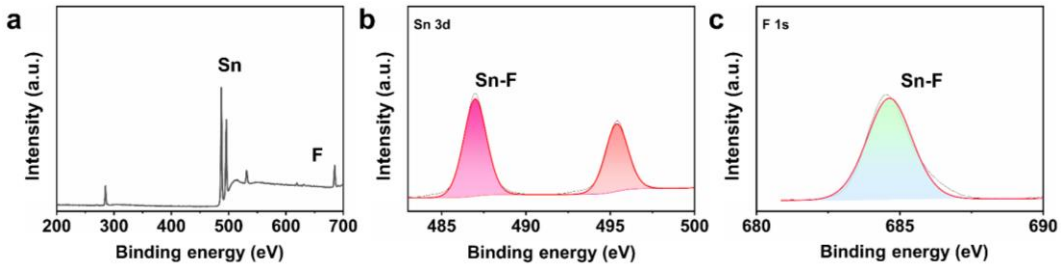

Figure S3. XPS (a) of Sn 3d (b) and F 1s (c) for nano-SnF_2.

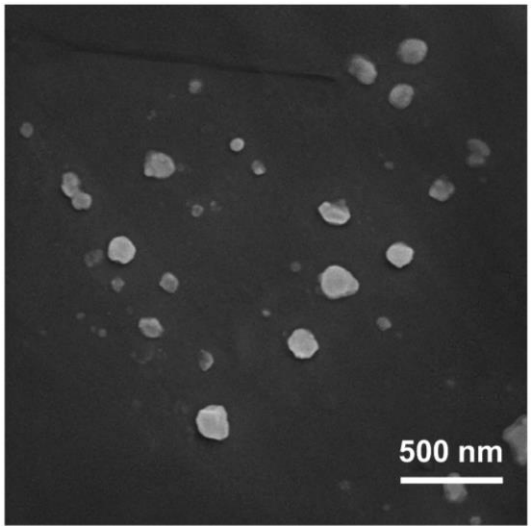

Figure S4. SEM image of nano-SnF_2.

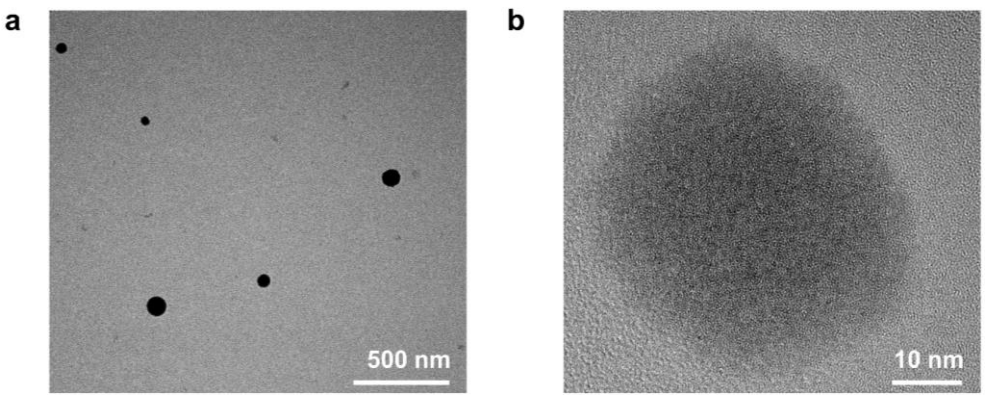

Figure S5. TEM images of nano-SnF_2.

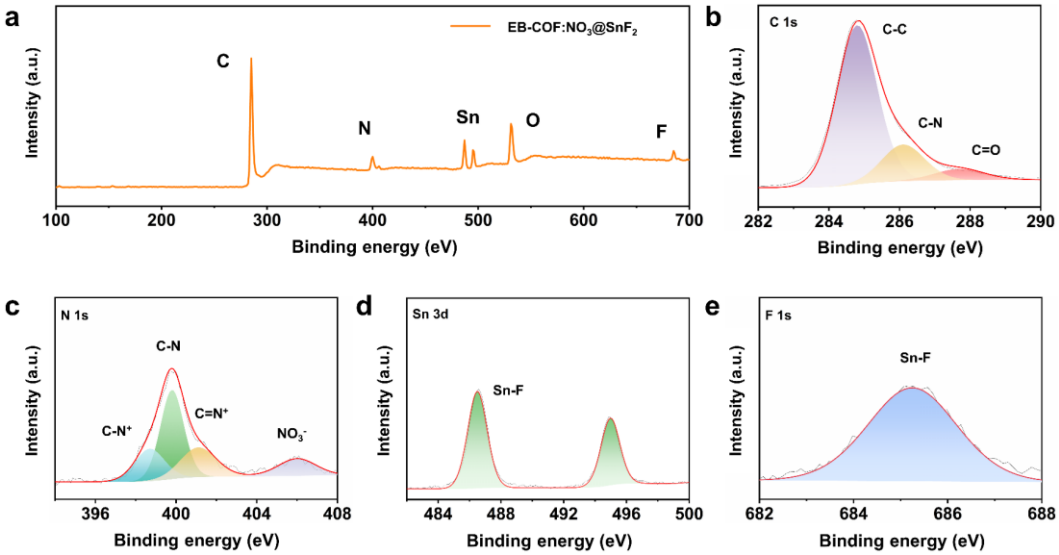

Figure S6. XPS (a) of C 1s (b) N 1s (c) Sn 3d (d) and F 1s (e) for EB-COF:NO_3@SnF_2.

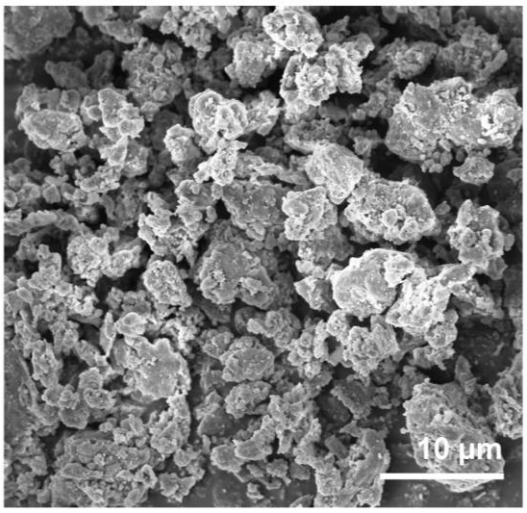

Figure S7. SEM image of EB-COF:NO_3@SnF_2.

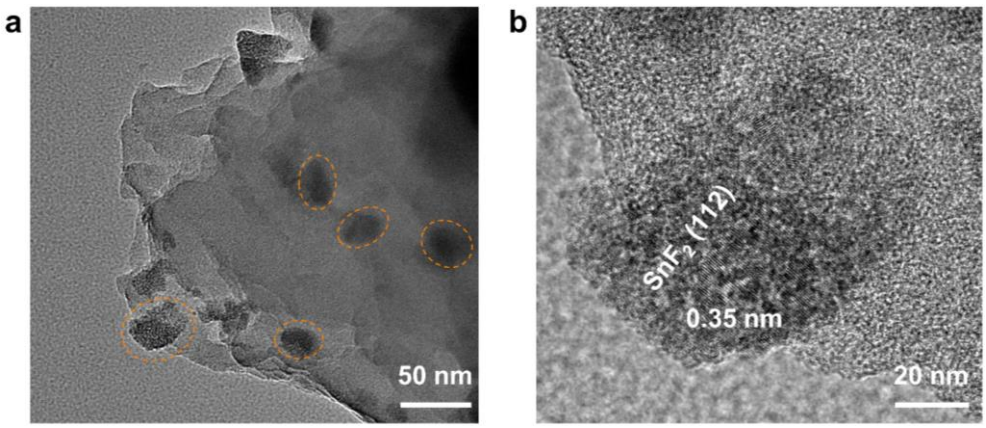

Figure S8. TEM image (a) and HRTEM image (b) of EB-COF:NO_3@SnF_2.

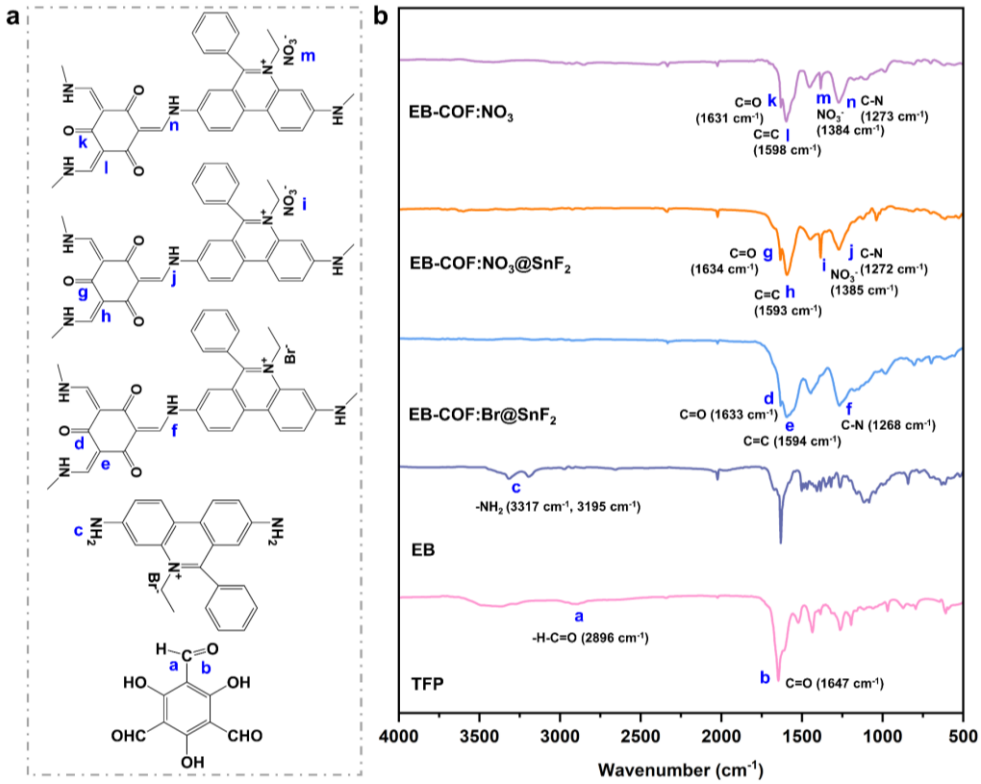

Figure S9. (a) The fragments of the chemical structure formula and (b) the FT-IR spectra of TFP, EB, EB-COF:Br@SnF_2, EB-COF:NO_3@SnF_2 and EB-COF:NO_3.

It can be seen that the FT-IR spectra of EB-COF:Br@SnF_2 exhibits the peaks of C=O (1633 cm^{-1}), C=C (1594 cm^{-1}) and C-N (1268 cm^{-1}) while the aldehyde group (-H-C=O, 2896 and 1647 cm^{-1}) of TFP and the amino group (-NH_2, 3317 and 3195 cm^{-1}) of EB disappear, indicating that the formation of this COF is based on the co-condensation reaction between the aldehyde group in TEP and the amino group in EB.[1,2]. After the ion exchange process, the EB-COF:NO_3@SnF_2 displays the same peaks except for the new peak of NO_3^- (1385 cm^{-1})[3] as EB-COF:Br@SnF_2, which suggests that the framework structure of the COF remains stable. Moreover, the EB-COF:NO_3 without SnF_2 also exhibits similar FT-IR spectra compared to EB-COF:NO_3@SnF_2, presenting C=O, C=C, NO_3^- and C-N at 1631, 1598, 1384 and 1273 cm^{-1}, respectively.

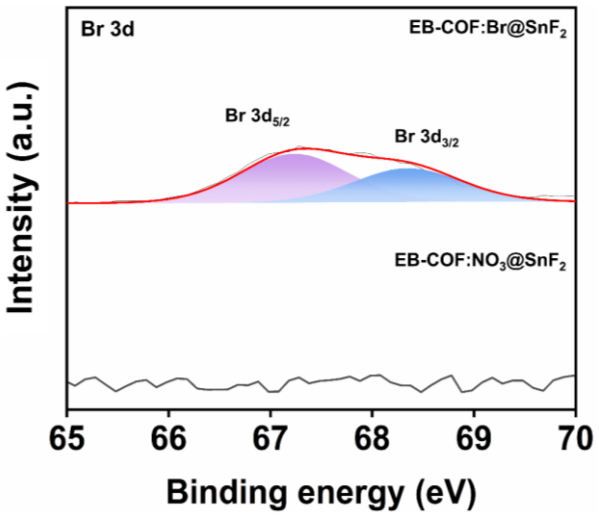

Figure S10. The XPS analyzation of Br 3d for EB-COF:Br@SnF_2 and EB-COF:NO_3@SnF_2.

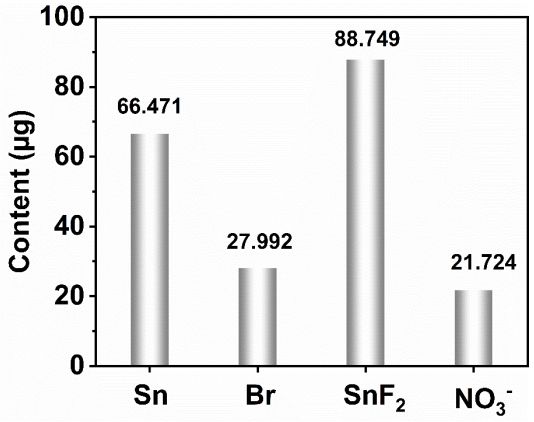

Figure S11. The ICP-MS results of Sn in EB-COF:NO_3@SnF_2 (1 mg) and Br in EB-COF:Br@SnF_2 (1 mg) and the calculated content of SnF_2 and NO_3^- in EB-COF:NO_3@SnF_2 (1 mg).

Fig. S11 demonstrates that 1 mg of EB-COF:NO_3@SnF_2 contains the element Sn (M = 118.71 g mol^{-1}) of 66.471 μg and 1 mg of EB-COF:Br@SnF_2 contains 27.992 μg of Br (M = 79.90 g mol^{-1}). Therefore, it can be calculated that 1 mg EB-COF:NO_3@SnF_2 contains 87.749 μg of SnF_2 (M = 156.71 g mol^{-1}) and 21.724 μg of NO_3^- (M = 62.01 g mol^{-1}).

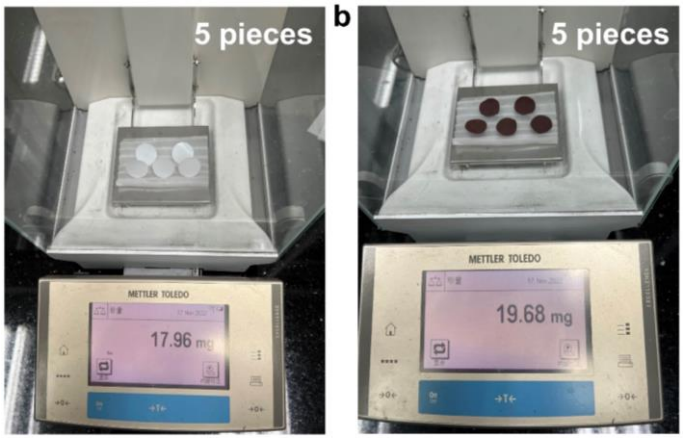

Figure S12. Optical photo of weighing (a) PP (Φ = 18 mm) and (b) PCS (Φ = 18 mm) mass.

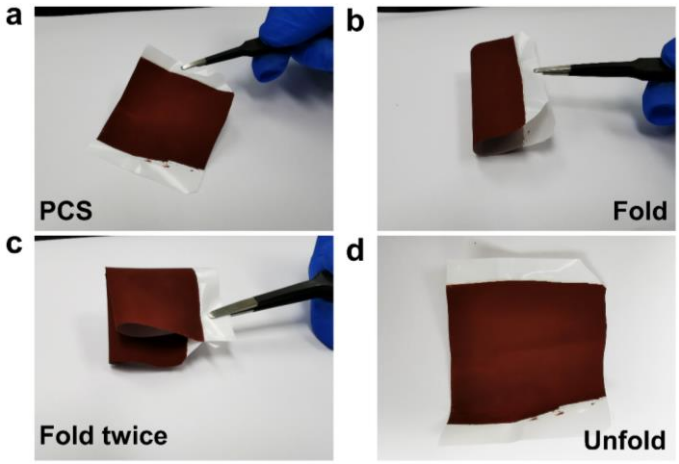

Figure S13. Optical photos of PCS in different states.

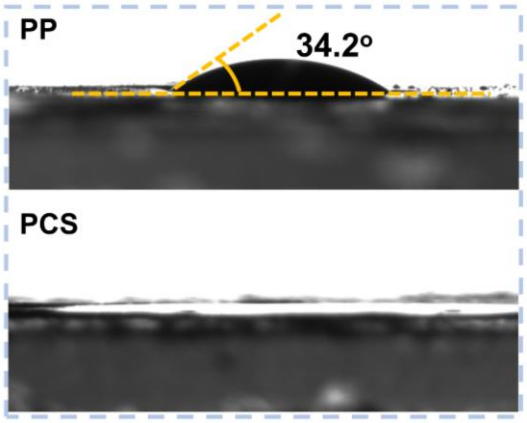

Figure S14. The contact angles between electrolyte and separators for PP and PCS.

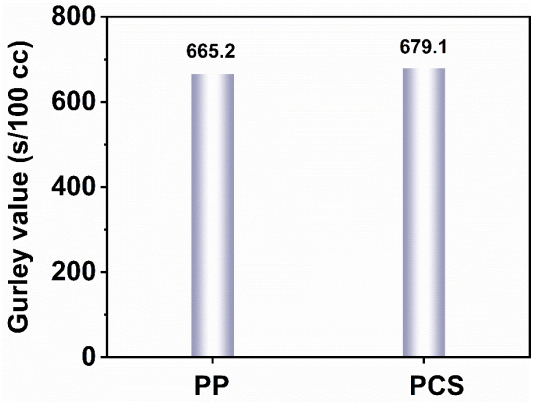

Figure S15. The Gurley value of PP and PCS.

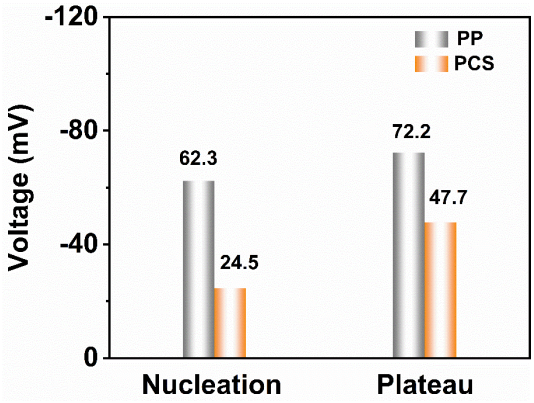

Figure S16. The measured nucleation overpotential and mass transfer-controlled plateau potential of the cell with PP and PCS.

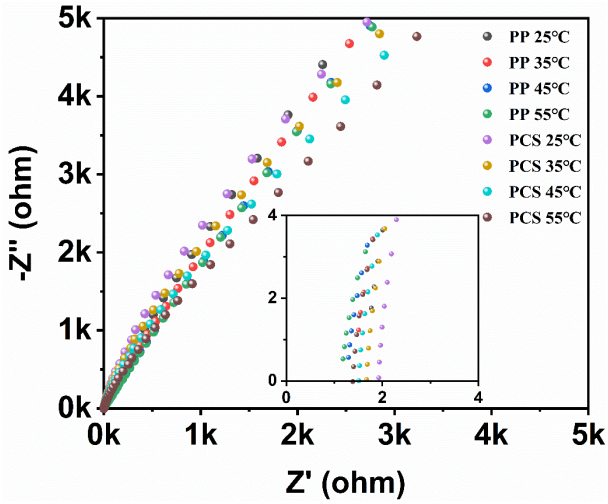

Figure S17. Electrochemical impedance spectra of symmetric stainless steel cells with PP and PCS under different temperature.

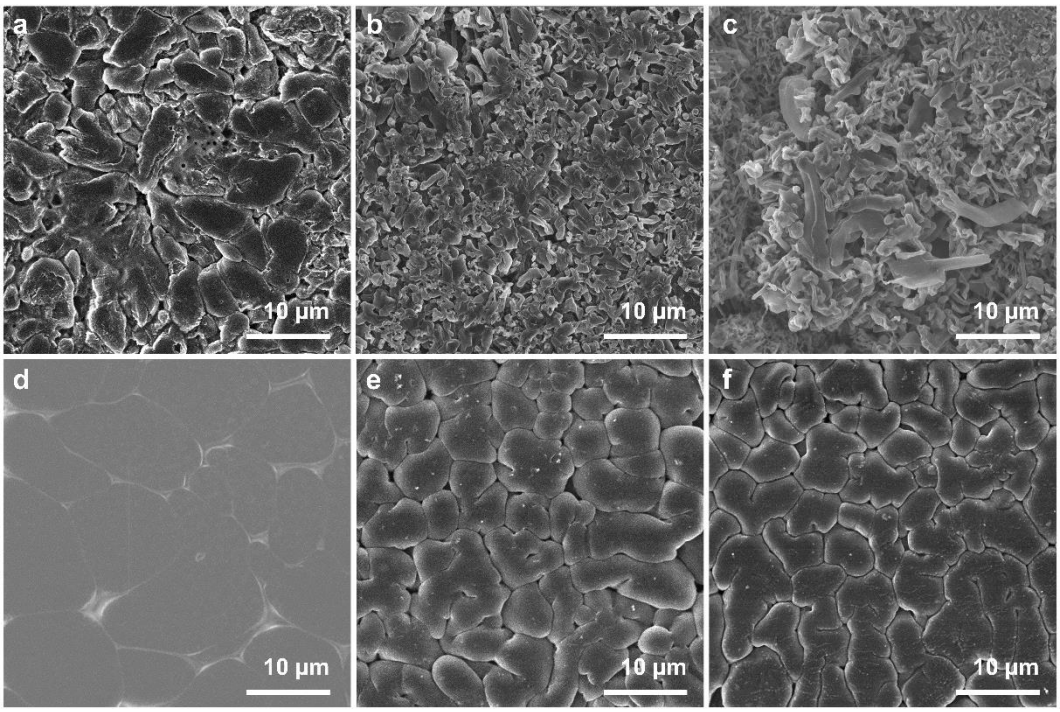

Figure S18. The SEM images of Li deposited with a fixed capacity of 4 mAh cm^{-2} using PP and PCS under different current densities of 0.5 (a and d), 2 (b and e) and 5 mA cm^{-2} (c and f), respectively.

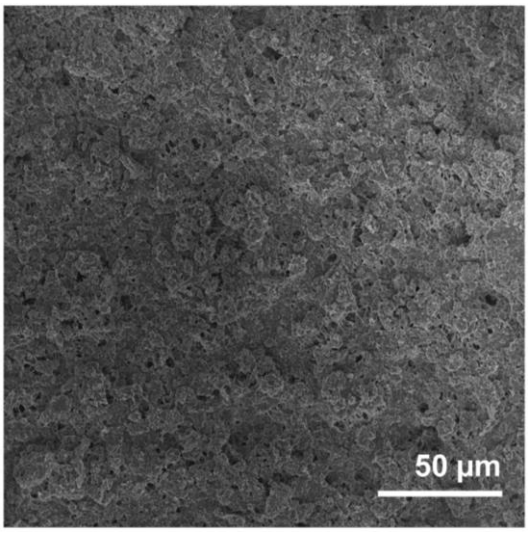

Figure S19. SEM image of PCS from Li//Cu cell after Li deposition process.

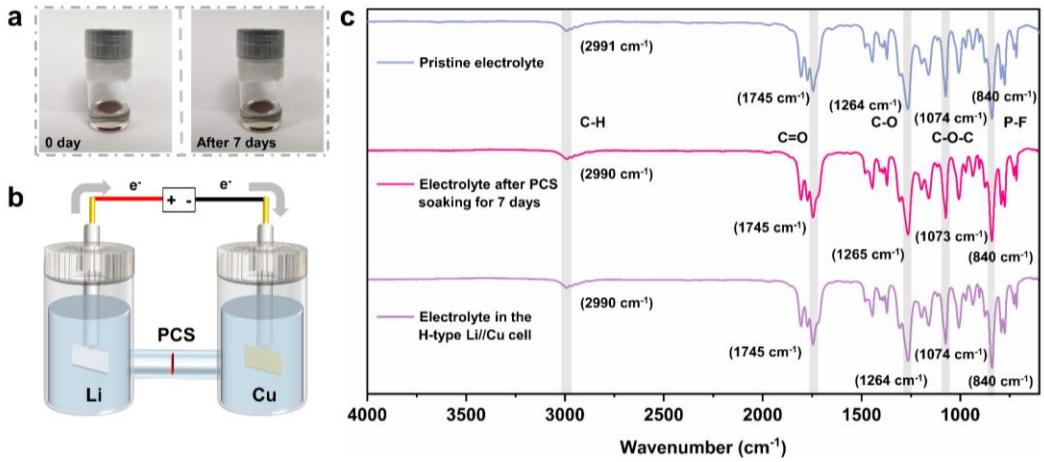

Figure S20. (a) Optical photos of electrolyte soaking PCS. (b) The H-type Li//Cu cell using PCS. (c) FT-IR spectra of pristine electrolyte and the electrolyte soaking PCS after 7 days and the electrolyte in H-type Li//Cu cell after Li deposition process.

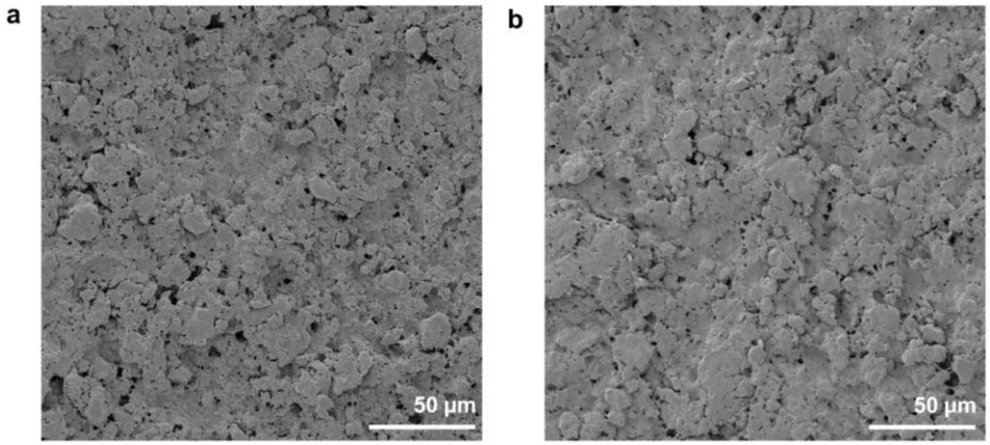

Figure S21. SEM images of PCS (a) before and (b) after soaking in electrolyte for 7 days.

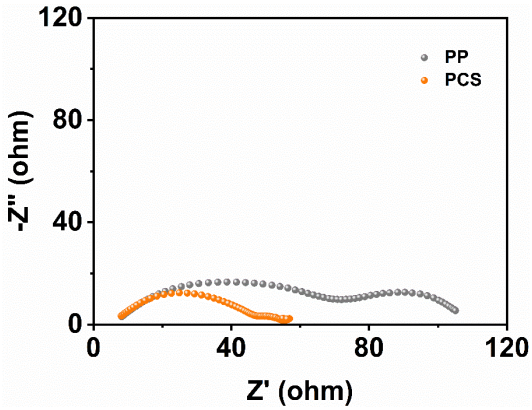

Figure S22. EIS spectra of Li symmetric cells with PP and PCS after 50 cycles under the current density of 1 mA cm^{-2} and the capacity of 1 mAh cm^{-2}.

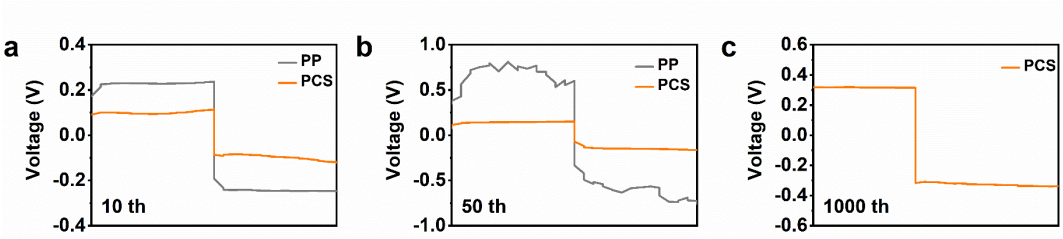

Figure S23. Galvanostatic voltage curves of Li symmetric cells with PP and PCS under the current density of 15 mA cm^{-2} for the areal capacity of 2 mAh cm^{-2} at (a) 10 th, (b) 50 th and (c) 1000 th cycles.

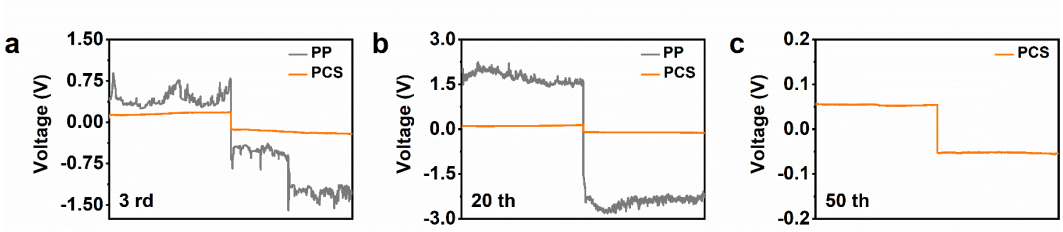

Figure S24. Galvanostatic voltage curves of Li symmetric cells with PP and PCS under the current density of 10 mA cm^{-2} for the areal capacity of 30 mAh cm^{-2} at (a) 3 rd, (b) 20 th and (c) 50 th cycles.

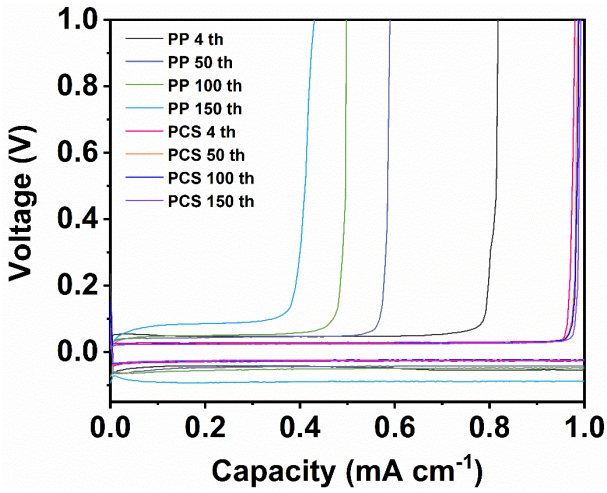

Figure S25. The selected voltage-capacity curve of Li//Cu cells with PP and PCS under the current density 1 mA cm^{-2} for the Li deposition capacity of 1 mAh cm^{-2}.

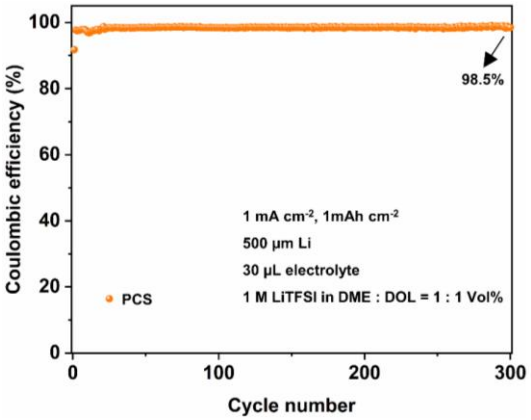

Figure S26. The coulombic efficiency of Li//Cu cell with PCS using ether-based electrolyte.

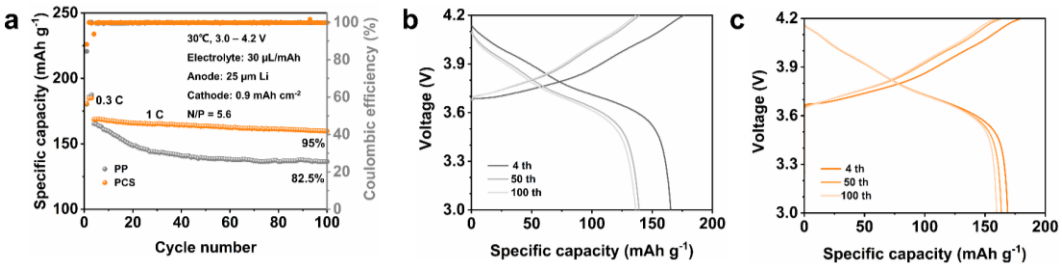

Figure S27. (a) Cycling performance and corresponding charge-discharge curves of Li//NCM811 full cells using (b) PP and (c) PCS with a voltage range of 3.0 - 4.2 V at 30℃.

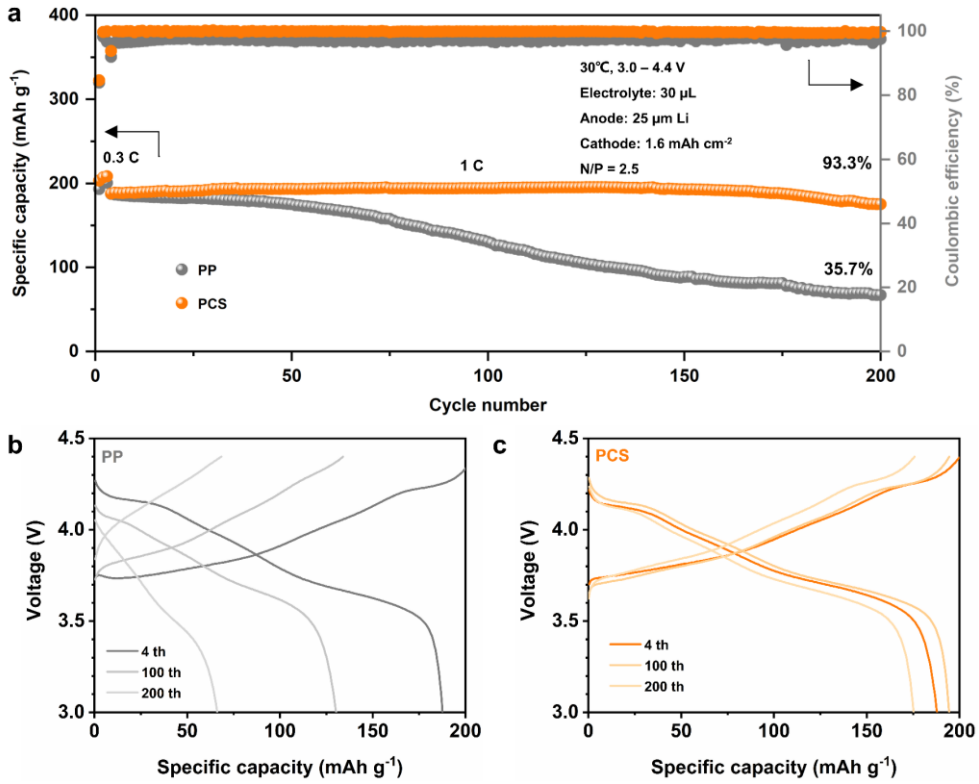

Figure S28. (a) Cycling performance and corresponding charge-discharge curves of Li//NCM811 full cells using (b) PP and (c) PCS with a voltage range of 3.0 - 4.4 V at 30°C.

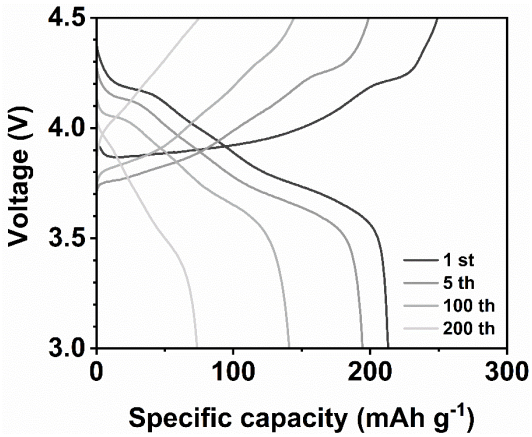

Figure S29. Selected charge-discharge curves of Li//NCM811 full cell using PP with a voltage range of 3.0 - 4.5 V at 30℃.

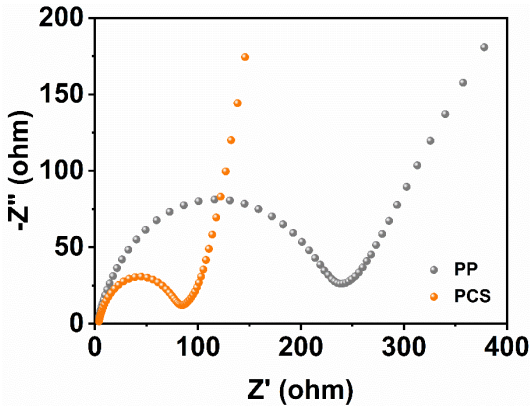

Figure S30. EIS spectra of Li//NCM811 full cells with PP and PCS after 50 cycles.

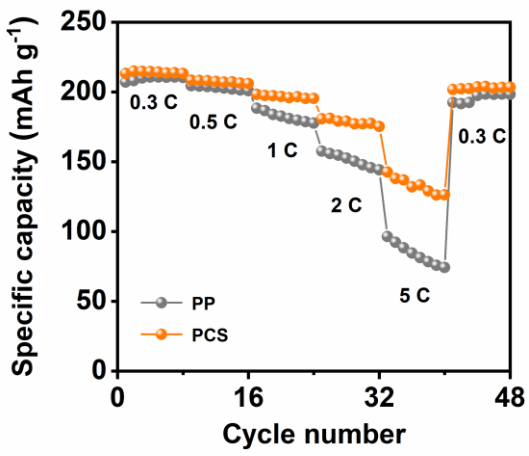

Figure S31. Rate performance of Li//NCM811 full cells using PP and PCS with a voltage range of 3.0 - 4.5 V at 30℃.

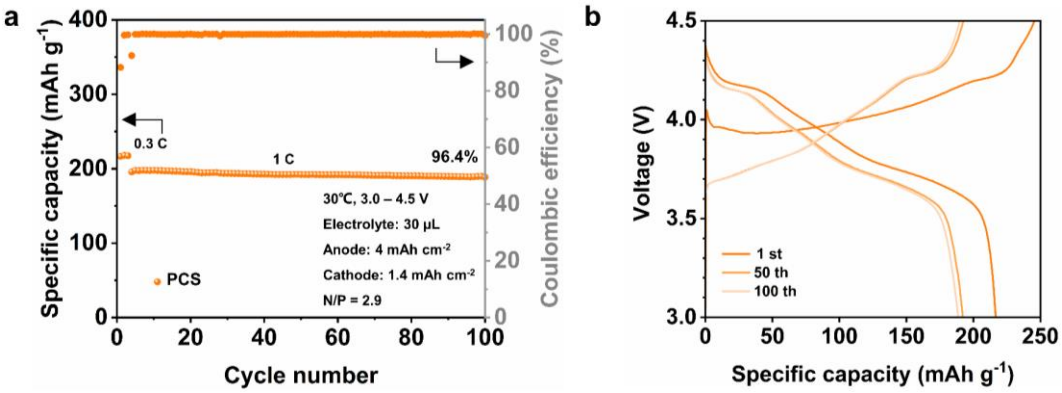

Figure S32. (a) Cycling performance and (b) selected charge-discharge curves of NCM811 full cell using Cu anode with pre-deposited Li (4 mAh cm^{-2}) under a voltage range of 3.0 - 4.5 V at 30℃.

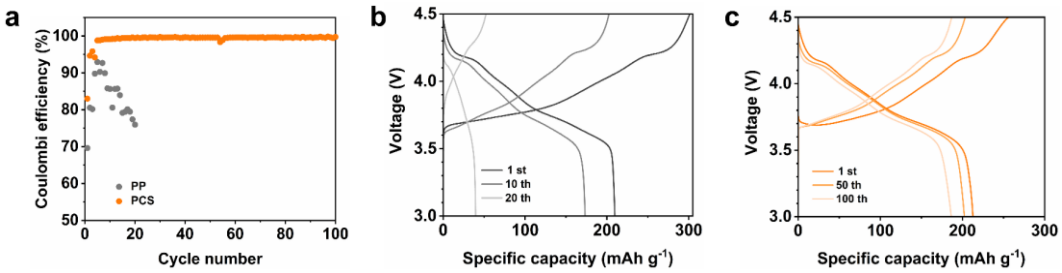

Figure S33. (a) The CEs and selected charge-discharge curves of Li//NCM811 full cells using (b) PP and (c) PCS with a voltage range of 3.0 - 4.5 V at 60℃.

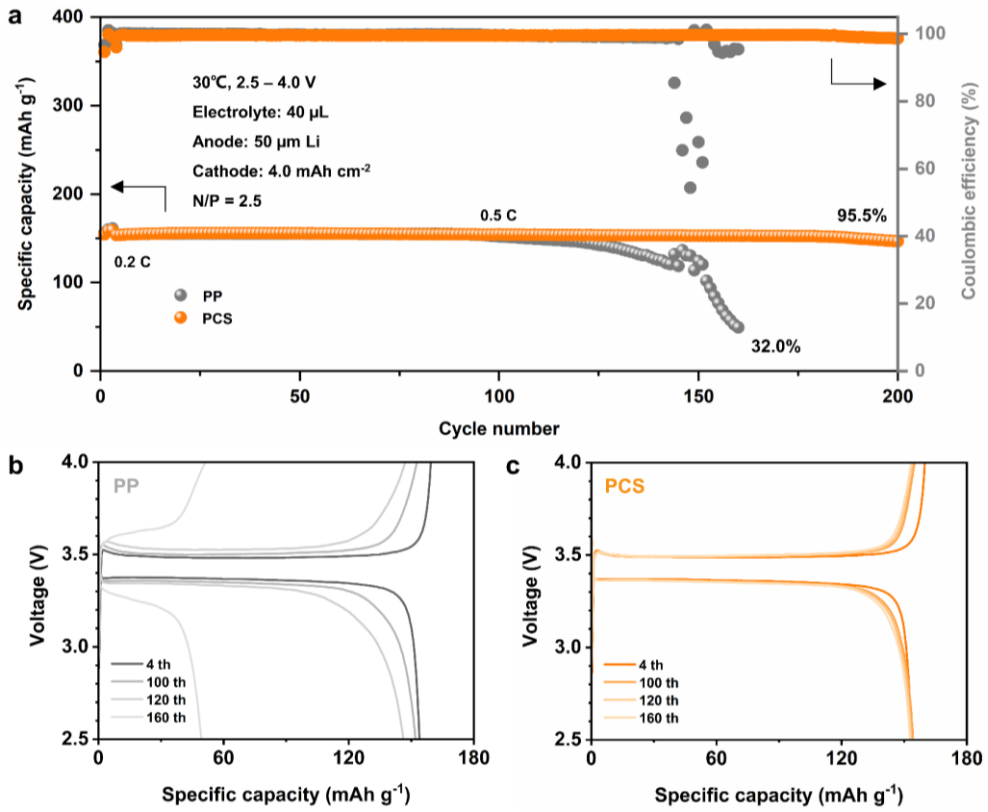

Figure S34. (a) Cycling performance and corresponding charge-discharge curves of Li//LFP full cells using (b) PP and (c) PCS with a voltage range of 2.5 - 4.0 V at 30℃.

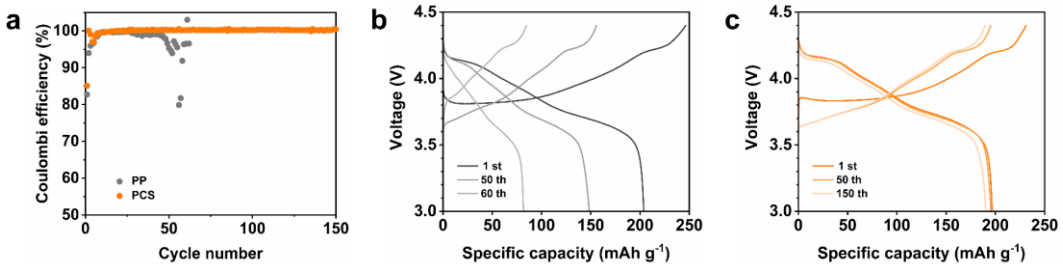

Figure S35. (a) The CEs and selected charge-discharge curves of Li//NCM811 full cells using (b) PP and (c) PCS with a voltage range of 3.0 - 4.4 V at 30℃.

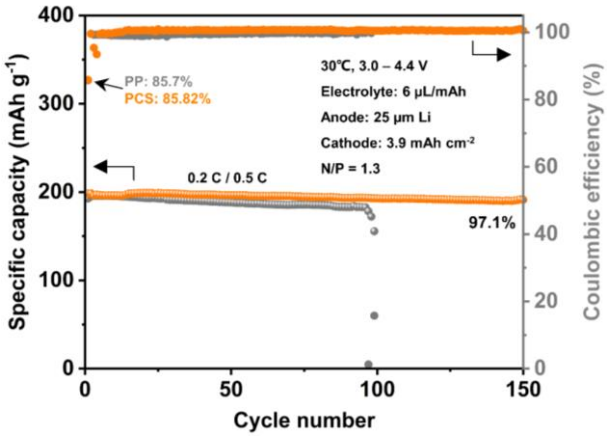

Figure S36. Cycling performance of Li//NCM811 full cells using PP and PCS in the other type of electrolyte (1.0 M lithium oxalyldifluoroborate (LiDFOB) in ethylene carbonate (EC) : ethyl methyl carbonate (EMC) = 3 : 7 in Vol% with 2% Fluoroethylene carbonate (FEC)) with a voltage range of 3.0 - 4.4 V at 30℃.

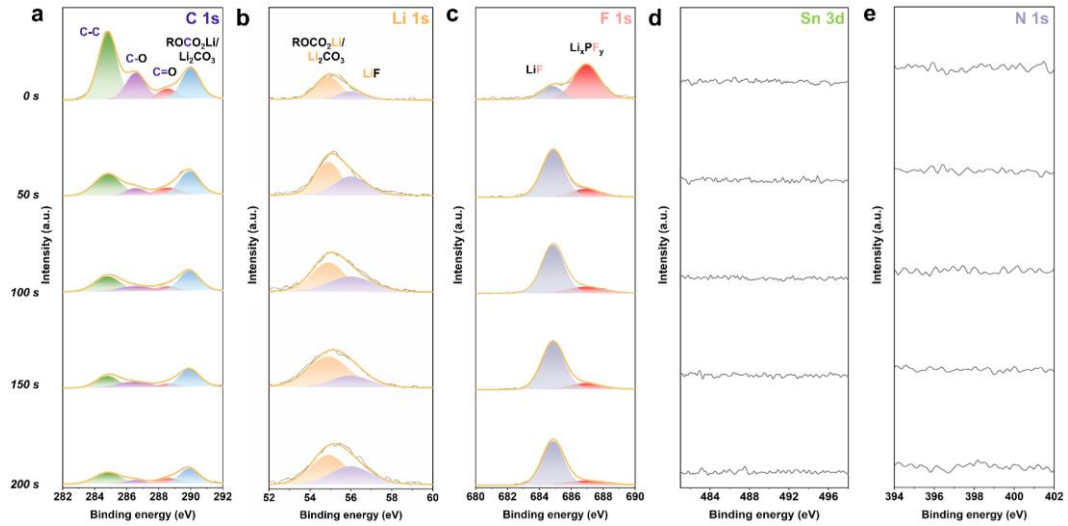

Figure S37. XPS analyzation of (a) C 1s, (b) Li 1s, (c) F 1s, (d) Sn 3d and (e) N 1s profiles for Li from Li symmetric cell using PP after cycling.

As shown in **Fig. S37a**, the C 1s spectra of Li using PP is dominated by the matters formed by the decomposition of electrolyte solvent, including C-C (284.8 eV), C-O (286.6 eV), C=O (288.6 eV) and Li_2CO_3/$ROCO_2Li$ (290.0 eV) during the etching process. Moreover, with the etching time, the peak of Li_2CO_3/$ROCO_2Li$ gradually dominates, which indicates that Li metal suffers from severe erosion of the electrolyte after cycling. The results of the Li 1s spectra can be regarded as evidence of the vigorous decomposition of the electrolyte, where Li 1s spectra exhibits the peaks of Li_2CO_3/$ROCO_2Li$ (54.9 eV) and LiF (56.0 eV), and the signals of peaks are clearly visible throughout the etching process (**Fig. S37b**). Moreover, the F 1s spectra reveals that $LiPF_6$ also experiences severe decomposition because LiF, as a decomposition product of $LiPF_6$, displays a strong signal across the etching operation (**Fig. S37c**). And regarding **Fig. S37d** and **e** no signal appears.

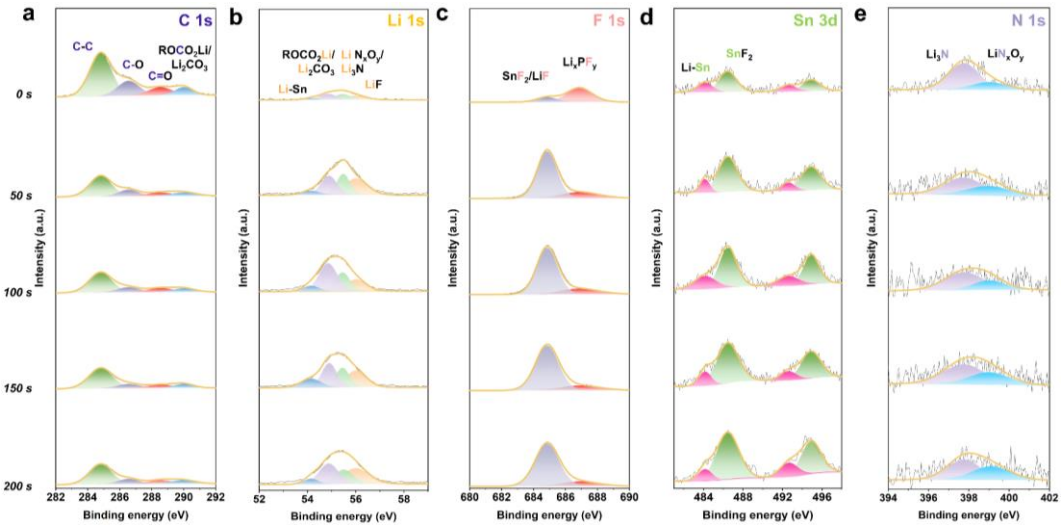

Figure S38 The XPS analyzation of (a) C 1s, (b) Li 1s, (c) F 1s, (d) Sn 3d and (e) N 1s depth profiles of Li from the other side (contacting with the surface of PP) of the Li symmetric cell with PCS after cycling.

Fig. S38a demonstrates that the surface of the cycled Li is populated by numerous organic compounds, including C-C, C-O, C=O, and Li_2CO_3/$ROCO_2Li$, which come from the decomposition of electrolyte solvents. And the signal gradually diminishes with the depth of etching, indicating that the outer layer of the SEI is enriched with more organic species. The Li 1s spectra demonstrates the peaks of LiF, Li_3N/LiN_xO_y, Li_2CO_3/$ROCO_2Li$ and Li-Sn, and presents a stronger signal relatively to the surface layer as the etching time progresses (**Fig. S38b**), suggesting that the inner layer of SEI enriches more inorganic material. The F 1s spectra displays a similar tendency with a significant accumulation of SnF_2/LiF (**Fig. S38c**). The appearance of the peak of Li-Sn in the Sn 3d spectra confirms the occurrence of the reaction between SnF_2 and Li, since the signal of Li-Sn is available throughout the etching process (**Fig. S38d**). Moreover,

during the entire etching process, the N 1s spectra is primarily dominated by Li_3N and LiN_xO_y (**Fig. S38e**), which results from the reduction of NO_3^- released in the PCS. According to the XPS results, an approximately characteristic profile of the SEI can be depicted. Its outer layer accumulates more organic substances caused by the decomposition of electrolyte solvents, and its inner layer contains more inorganic substances such as LiF, Li_3N/LiN_xO_y, $Li_2CO_3/ROCO_2Li$ and Li-Sn. It is similar to the XPS results of the Li electrode (contacting with the surface of the coating) from the Li symmetric cell in **Fig. 5e-i**.

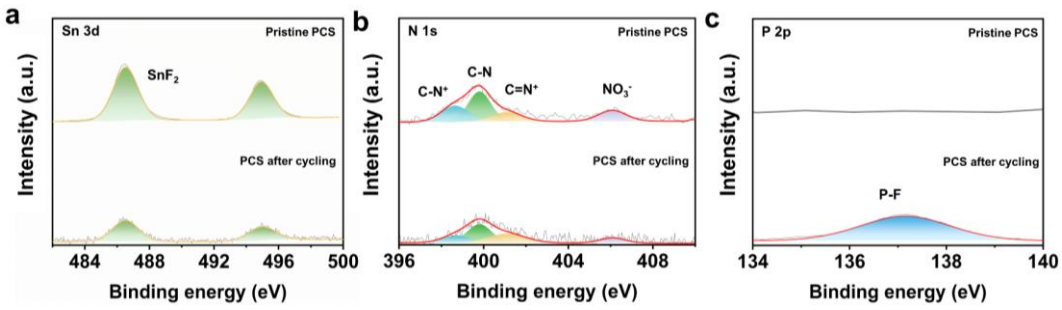

Figure S39. The XPS analyzation of (a) Sn 3d (b) N 1s and (c) P 2p for PCS from Li symmetric cell before and after cycling.

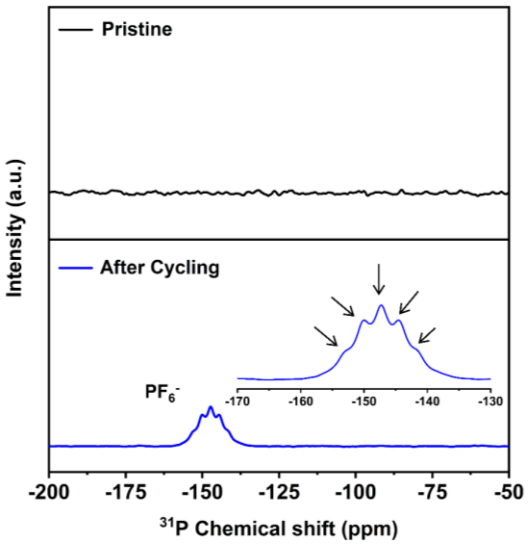

Figure S40. The solid-state ^{31}P NMR spectrum of PCS before and after 100 cycles.

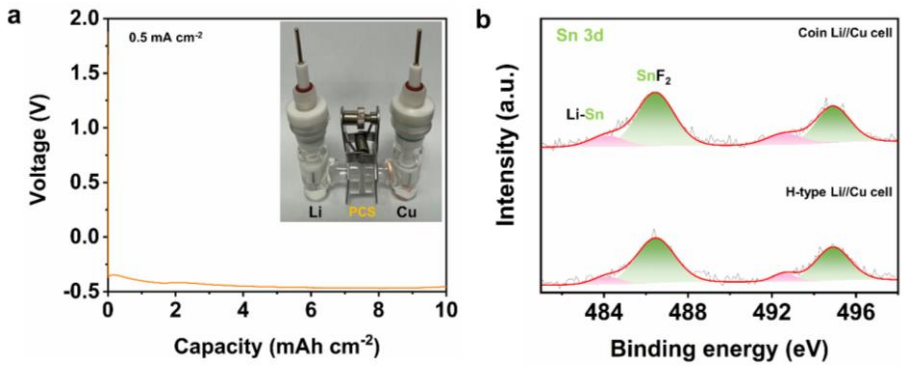

Figure S41. (a) The galvanostatic voltage profiles and optical photograph (insert) of the H-type cell with PCS under a current density of 0.5 mA cm^{-2} and a capacity of 10 mAh cm^{-2}. (b) The XPS analyzation of Sn 3d for Cu from coin and H-type Li//Cu cell after Li deposition process.

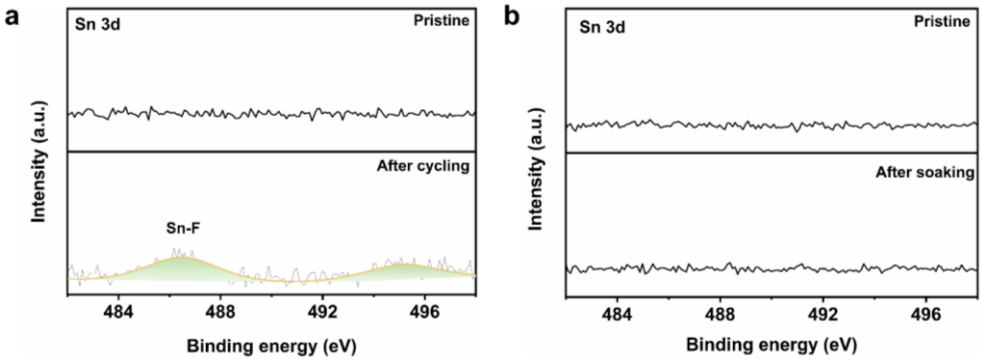

Figure S42. (a) XPS of the uncoated side of the PCS from symmetric Li metal cell before and after cycling. (b) XPS of the uncoated side of the PCS before and after soaking in electrolyte.

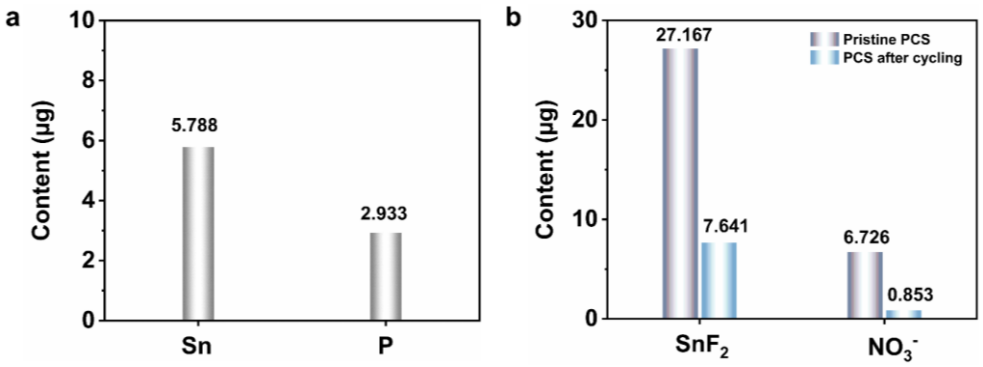

Figure S43. (a) The ICP-MS result of Sn and P element in PCS from Li//NCM811 full cell after 200 cycles. (b) The content of SnF_2 and NO_3^- in PCS from Li//NCM811 full cell before and after 200 cycles.

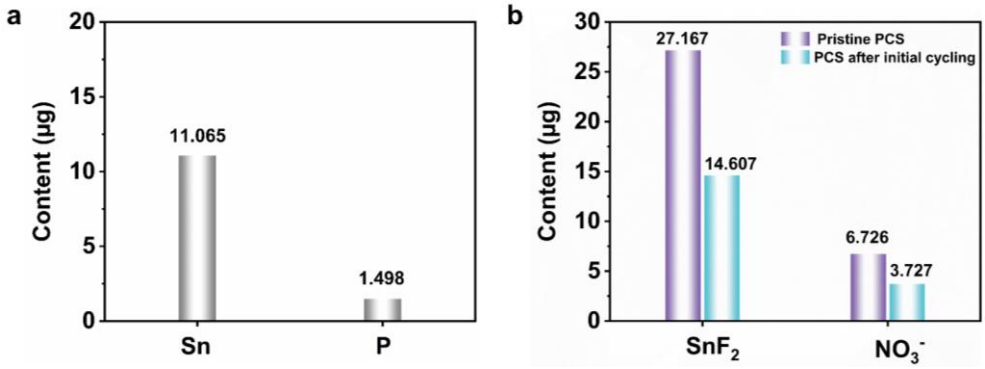

Figure S44. (a) The ICP-MS result of Sn and P element in PCS from Li//Cu cell after the initial cycling. (b) The content of SnF_2 and NO_3^- in PCS before and after the initial cycling.

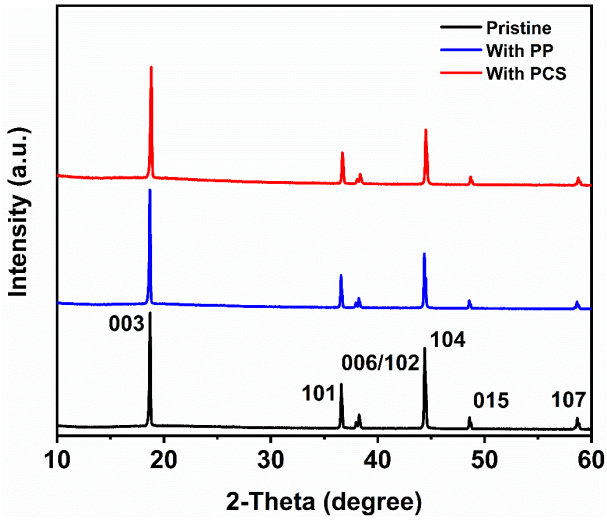

Figure S45. XRD results of the NCM811 electrodes using (a) PP and (b) PCS after 30 cycles with a voltage range of 3.0 - 4.4 V.

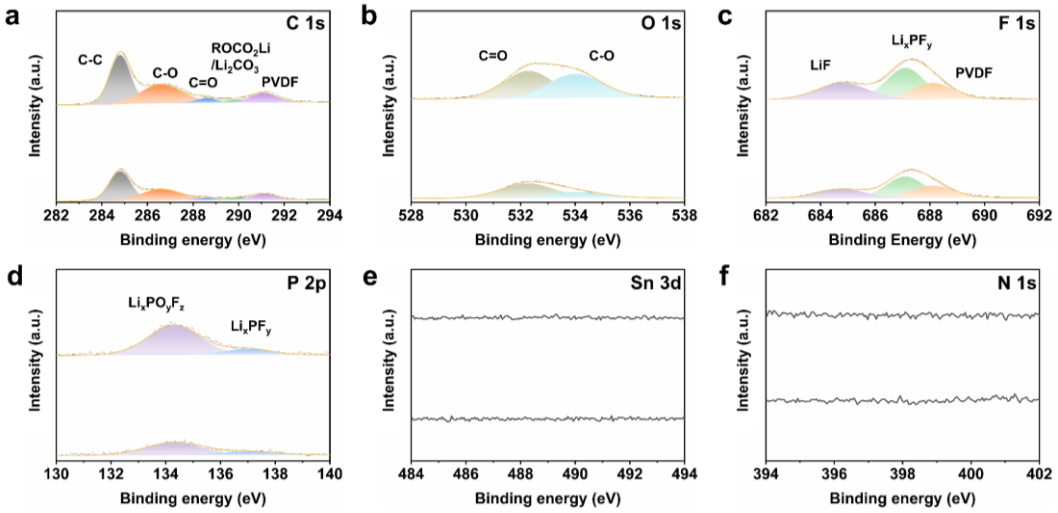

Figure S46. XPS analyzation of (a) C 1s, (b) O 1s, (c) F 1s, (d) P 2p, (e) Sn 3d and (f) N 1s for NCM811 electrode with PP (top) and PCS (bottom) after cycling.

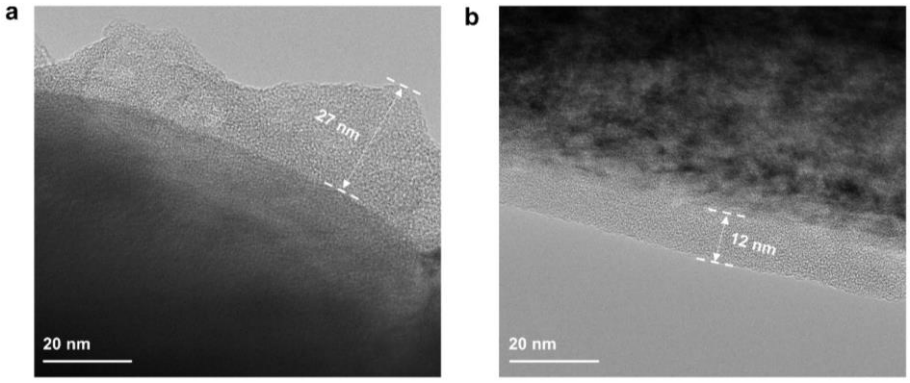

Figure S47. TEM images of NCM811 with (a) PP and (b) PCS after cycling.

Table S1. Performance comparison between PCS and other functionalized separators reported from literatures.

Maximum current density (mA cm^{-2})	Maximum areal capacity (mAh cm^{-2})	Ref
15	2	This work
10	30	
5	5	4
0.5	5	37
1	1	38
1	1	39
2	2	40
10	10	41
0.2	1	42
1	1	43
3	1	44
5	5	45
5	10	46
0.65	0.65	47
3	1	48
5	1	49
20	5	50
1	1	51
0.5	1	52
5	5	53
8.2	5.47	55

Table S2. The calculation result related to the capacity loss caused by PCS after the initial cycling.

Cell type	(Φ = 15.6 mm) Li//Cu		
Current density (mA cm^{-2}) and deposition time (h)	1; 2		
Total Li capacity (mAh)	3.82		
Measured initial irreversible capacity loss (%)	9.2		
Loss species	SnF_2		NO_3^-
Loss content (μg)	13.097		2.999
Converted species	Li_5Sn_2	LiF	Li_3N
Loss Li capacity (mAh)	0.00560	0.00448	0.00389
Loss Li capacity ratio (%)	0.147	0.117	0.102
Total loss Li capacity ratio (%)	0.366		

The loss of Li capacity (C_{Loss}) was calculated according to the following equation.

$$C_{Loss} = (m / M) \times r \times M_{Li} \times C_{Li}$$

Where m represents the reduced mass of SnF_2 or NO_3^-, M represents the molar mass, r represents the ratio of atomic numbers (2.5, 2 and 3, respectively), M_{Li} represents the molar mass of Li (6.94 g mol^{-1}) and C_{Li} represents the specific capacity of Li (3860 mAh g^{-1}).

1 S. Kandambeth, A. Mallick, B. Lukose, M. V. Mane, T. Heine, and R. Banerjee, *J. Am. Chem. Soc.*, 2012, **134**, 19524-19527.

2 H. Ma, B. Liu, B. Li, L. Zhang, Y.-G. Li, H.-Q. Tan, H.-Y. Zhang, and G. Zhu, *J. Am. Chem. Soc.*, 2016, **138**, 5897-5903.

3 X. Xue, F. Yu, J.-G. Li, G. Bai, H. Yuan, J. Hou, B. Peng, L. Chen, M.-F. Yuen, G. Wang, F. Wang, and C. Wang, *Int. J. Hydrogen Energy*, 2020, **45**, 1802-1807.